



# Implementation of Water Tracers in the Met Office Unified Model

Alison J. McLaren<sup>1</sup>, Louise C. Sime<sup>1</sup>, Simon Wilson<sup>2</sup>, Jeff Ridley<sup>3</sup>, Qinggang Gao<sup>1</sup>, Merve Gorguner<sup>4</sup>, Giorgia Line<sup>3</sup>, Martin Werner<sup>5</sup> and Paul Valdes<sup>4</sup>

- <sup>1</sup>Ice Dynamics and Palaeoclimate, British Antarctic Survey, Cambridge, U.K.
- 5 <sup>2</sup>National Centre for Atmospheric Science, Computational Modelling Service, University of Reading, U.K.
  - <sup>3</sup>Met Office Hadley Centre, Exeter, U.K.
  - <sup>4</sup>School of Geographical Sciences, University of Bristol, U.K.
  - <sup>5</sup>Alfred Wegener Institute, Helmholtz Centre for Polar and Marine Research, Bremerhaven, Germany
- 10 Correspondence to: Alison McLaren (aliren@bas.ac.uk)

#### Abstract.

There is an increasing need to understand how water is cycled and transported within the atmosphere to aid water management. Here, atmospheric water tracers are added to the Met Office Unified Model (UM) to allow tracking of water within the model. This requires the implementation of water tracers in the following parts of the model code: large-scale advection, surface evaporation, boundary layer mixing, large-scale precipitation (microphysics), large-scale clouds, stochastic physics and convection. A single water tracer is found to track all water in the model to a high degree of accuracy during a 35-year simulation; the differences are typically less than  $10^{-16}$  kg kg<sup>-1</sup> at the end of every timestep, prior to a very small adjustment to prevent the build up of numerical error. The increase in computing time for each water tracer is between 3.1 and 3.8% depending on the model resolution. The model development is tested by using the water tracers to find the sources of precipitation in a historical UM simulation. As expected, the majority of precipitation is found to be sourced directly from the ocean, with the recycling of water over land becoming increasingly important downwind across continents. The UM results for the mean evaporative source properties of precipitation are comparable to those of the ECHAM6 atmospheric model, with some interesting local differences over Antarctica, Greenland and the Indian monsoon region. Finally, the components of the model's global hydrological cycle that can be derived from the water tracers are presented to illustrate the additional information that can be provided from the new development.

## 1 Introduction

A major part of the global hydrological cycle consists of water evaporating at the surface, being transported through the atmosphere, and eventually returning to the surface as rain or snow. The water vapour in the atmosphere has a mean residence time of 8-10 days (Gimeno et al., 2021) and during this time it can be advected thousands of kilometres (e.g. Fiorella et al.,





2021). Thus, the moisture source and sink locations for precipitation can differ greatly. For water management purposes, it is becoming increasingly important to understand how water moves through the atmosphere between regions, at global and regional scales, and how it may change in the future (Rockström et al., 2023). This is because humans are affecting the water cycle both directly, via processes such as extraction and irrigation, and indirectly through climate change and land surface changes (Abbott et al., 2019; Allan et al., 2020; Dorigo et al. 2021).

Gimeno et al. (2012) reviewed the various methods for tracking atmospheric water pathways, which they divided into three groups: analytical/box models, numerical water vapour tracers, and physical water vapour tracers (i.e. water isotopes). The numerical tracer approach has been used in 'offline', using an Eulerian or Lagrangian framework, and 'online' models (Dominguez et al., 2020). 'Offline' systems use water tracking models forced by output from General Circulation Models (GCMs) or reanalyses (e.g. Tuinenburg et al., 2020; van der Ent et al., 2010, 2014). 'Online' models involve embedding numerical water tracers (hereafter termed 'water tracers') into a GCM and is the focus of this paper. The online method allows a greater complexity in the representation of the processes that affect water (Dominguez et al., 2020), plus it has the advantage that the tracers respond to their forcing at every model timestep rather than using time-averaged offline fields. However, this comes with the added computational cost of running a GCM, although recent water tracer developments have made the method more efficient as discussed below. Including online water tracers in climate model simulations also allows predicted changes in water transport to be easily investigated.

Water tracers track moisture around a GCM and are impacted by the same physical processes that affect water in the model. However, unlike the model's prognostic water fields, they are passive tracers in that they do not affect the physics or dynamics of the model. Water tracers, including water isotopes, have been successfully added to many GCMs (recent examples include Nusbaumer et al., 2017, and Cauquoin et al., 2019) following the early work of Joussaume et al. (1984) and Koster et al. (1986). Stable water isotopes can be viewed as a special type of water tracer that undergo fractionation during phase changes. Typically, non-isotopic water tracers have been used to track the source region of precipitation by tagging water evaporating from prescribed regions. This technique has been used to investigate the sources of Antarctic and Greenland precipitation to aid the interpretation of ice core isotopic measurements (e.g. Werner et al., 2001; Delaygue et al., 2000; Noone and Simmonds, 2002). Outside of the polar regions, water tracers have been used to investigate precipitation source regions including over the Indian Monsoon region (Tharammal et al., 2023), the Eurasian continent (Numaguti, 1999), North America and India (Bosilovich and Schubert, 2002) and during an atmospheric river over North America (Nusbaumer and Noone, 2018). Following the nomenclature of Gao et al. (2024; hereafter 'G24'), this type of water tracer is termed here as a 'prescribed region' tracer.

Recently, Fiorella et al. (2021) introduced 'process-orientated' water tracers which included a water tracer that captures the precipitation weighted mean value of an evaporative property (e.g. latitude or sea surface temperature, SST). G24 further



75



developed this method to focus on ocean sourced precipitation and to ensure water tracer conservation; they used the scheme to look at investigate ocean source properties of Antarctic precipitation in the ECHAM6 model. Following G24, these tracers are referred to here as 'scaled-flux' tracers to distinguish them from the prescribed region tracers. A comparison between prescribed region and scaled-flux tracers is presented in G24. In summary, the scaled-flux tracer produces a more precise estimate of the mass weighted mean evaporative property in a highly efficient way compared with the prescribed region method. Therefore, using these online tracers to find the mean location of evaporative sources of precipitation has become less computationally expensive. The disadvantage of the scaled-flux method is that it does not capture any information about the variability of the source property. However, analysing mean values over short timescales (e.g. daily data) does provide some information on the variability.

This paper describes the implementation of non-isotopic water tracers in the Met Office Unified Model (Brown et al., 2012). The UM is an operational atmospheric model used across a range of timescales from weather to climate; it is the atmospheric component of the UK Earth System Model (UKESM; Sellar et al., 2019). The UM water tracer development is the first stage of a larger project to add water isotopes to the UKESM. As noted by Noone and Sturm (2010), implementing water tracers in a GCM comprises most of the effort required for adding isotopes to a GCM. Water isotopes were added to an earlier version of the UM as part of the work by Tindall et al. (2009) to include water isotopes in the coupled model HadCM3 (Pope et al., 2000; Gordon et al., 2000); HadCM3, which is relatively computationally efficient to run, continues to be well used by the palaeoclimate community (Valdes et al, 2017; Oger et al, 2023). However, the isotope code written for HadCM3 was never permanently included in the UM, and is therefore, out of date with more recent UM versions. Hence, in order to add water tracers and isotopes to the state-of-the-art model version, the UM code development described here is brand new. A key

priority of the work is to ensure water tracers (and eventually water isotopes) become a permanent option in the UM to ensure

The purpose of this paper is to document the UM water tracer implementation and to provide evidence that the scheme is working as expected. For a general description of how water tracers and isotopes are added to a GCM, the reader is referred to Noone and Sturm (2010). The paper is structured as follows. The water tracer implementation is described in section 2, together with an assessment of the computing cost of the water tracers. Definitions of the different types of water tracers are also provided in Section 2, plus details of the simulations used to test the development. Section 3 contains the results from the test simulations including a comparison with the ECHAM6 atmospheric model. The paper ends with conclusions in section 4.

95

90

the longevity of this development.



100

105

110

120



# 2 Model Description

The UM solves the non-hydrostatic, fully compressible deep-atmosphere equations of motion using a semi-implicit semi-Lagrangian method (Wood et al., 2014). The model uses a regular longitude-latitude grid with terrain-following hybrid height coordinates. The 'Global Atmosphere' (GA) 7.0/7.1 science configuration of the UM is documented in Walters et al. (2019). The most recent scientific configuration (GAL9.0, Willett et al., 2024) is used in this study. The UM is run with the Joint UK Land Environment Simulator (JULES) land surface model (Best et al., 2011; Clark et al., 2011). However, in this study, water tracers are not included in JULES and remain in the atmosphere component only.

## 2.1 Basic Water Tracer Code Development

Water tracers are added to the UM such that they evolve according to the same processes that act on the model's prognostic water fields, with the aim of following the model's water as precisely as possible. This requires adding water tracers to the following schemes: large-scale advection, surface evaporation, boundary layer mixing, large-scale precipitation (microphysics), large-scale clouds, stochastic physics and convection. Unlike water, the water tracers are passive and do not impact on the model physics or dynamics. The water tracers are held in an array with the number of water tracers set by the user. The first water tracer in the array mimics the prognostic water in the model and is named here as the 'normal water tracer'. This tracer is used to continually test the water tracer simulation as it can be compared directly to the model's water fields. The other water tracers in the array can then be used to trace specific water around the model or water properties (e.g. prescribed-region or scaled-flux tracers), and, in the future, to model water isotopes.

In the UM configuration used here, water is modelled using four prognostic fields for vapour, liquid condensate, ice condensate and large-scale rain (see Walters et al., 2019, for details); note, snow remains purely a diagnostic quantity. Equivalent prognostic fields for water tracers are defined as the product of the water field and the ratio of the water tracer to water. For example, the water tracer specific humidity equivalent ( $q_{wt}$ ) is

$$q_{wt} = R_q q \tag{1}$$

where  $R_q$  is the ratio of water tracer vapour to water vapour and q is the specific humidity. Water tracer fields for the other three water phases are similarly defined; therefore, adding m water tracers to the model requires an additional 4\*m tracer fields.

When water changes phase in the model, the water tracers are updated using the water tracer to water ratio of the source phase. For condensation as an example, the water tracers are updated as



130

135

140

145

150

155



$$q_{wt}^{n+1} = q_{wt}^n - R_q \Delta q \tag{2}$$

$$qcl_{wt}^{n+1} = qcl_{wt}^n + R_q \Delta q (3)$$

Where  $\Delta q$  is the change in q due to condensation,  $qcl_{wt}$  is the water tracer specific liquid condensate. n and n+1 indicate the values before and after the phase change respectively.

The large-scale advection of water tracers uses the same methods as prognostic water. In the model configuration used here, the semi-Lagrangian interpolation to the departure points uses a bi-cubic interpolation in the horizontal and a cubic Hermite interpolation in the vertical (Walters et al., 2019). Mass conservation of moist prognostics is enforced globally using the Optimised Conservative Filter (OCF) scheme of Zerroukat and Allen (2015) and the same scheme is used for the normal water tracer. Vertical transport of the water tracers in the convection and microphysics scheme is calculated as the relevant water tracer to water ratio multiplied by the water flux.

The water tracer code generally involves replicating the model's prognostic water code for the array of water tracers. For example, the water tracers pass through the entire convection and microphysics schemes following the vertical transport of water and undergoing the same phase changes. The water tracers are mostly updated in separate new subroutines to avoid overcomplicating the base model code. This means that the order of calculations for water tracers can be slightly different to water which due to numerical error will cause tiny differences between the normal water tracer and water. At the end of a timestep, the difference is typically less than  $10^{-16}$  kg kg<sup>-1</sup> when using double precision. Although this is an insignificant amount, this can grow quickly over time and hence a very small adjustment is made to the water tracers at the end of each timestep so that the normal water tracer exactly matches the equivalent water field. To ensure that this adjustment does not hide any issues, the code also contains a check to ensure that this adjustment remains less than  $10^{-10}$  kg kg<sup>-1</sup> over a timestep. In the 35-year long simulation that is used in this paper, the adjustment remains less than this level at every timestep showing that the water tracer code is correctly tracing the water in the model to a high degree of accuracy.

The water tracer code was included in UM release 13.2 in March 2023 following the code passing the Met Office code review process (Met Office Simulations Systems Working Practices, 2024). At this stage, normal water tracers were available to be used in runs using the GA 8.0 scientific configuration (Xavier et al., 2024). Since then, the code has been further developed in branches to: a) work with the Global Atmosphere Land 9.0 (GAL9.0) configuration (Willett et al., 2024), which will be the basis for the scientific configuration used in the simulations provided to the Coupled Model Intercomparison Project 7; and b) set up the prescribed region and scaled-flux types of water tracers as described in section 2.3.





#### 160 2.2 Computational Cost of Water Tracers

To assess the increase in computing cost caused by adding water tracers, month-long simulations with varying numbers of normal water tracers were run on the Met Office Cray XC40 supercomputer. Simulations were carried out at two resolutions: 'N96' which has a mid-latitude resolution of 135 km; and the higher resolution 'N216', with the mid-latitude grid spacing of 60 km. The N96 simulations were run with 0, 1, 3, 10, 23 and 50 water tracers, whilst the N216 simulations used a smaller subset of 0, 1, 3 and 23 tracers to reduce costs. These particular numbers of water tracers were tested as 3 tracers are typically used in water isotope enabled models, 23 are used in the experiment analysed below and 50 is an arbitrary large number. As the computing time can vary due to other factors (e.g. demand on the system, network variability), each experiment was repeated three times and the mean values are used here.

170

165

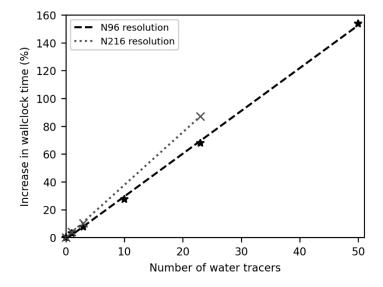


Figure 1: Increase in wallclock time (%) due to changing the number of normal water tracers in the simulation with lower resolution (N96, black stars) and higher resolution (N216, grey crosses) experiments. The linear fit of the results is shown by the black dashed line (N96) and dotted grey line (N216).

175

180

The wallclock time increases linearly with the number of water tracers (Fig. 1), with each additional water tracer increasing the computing time by 3.1% for N96 and 3.8% for N216 on average. Therefore, the water tracers are relatively efficient, mainly as there are computationally expensive areas of the UM that they do not impact (e.g. radiation, aerosols, cloud observation simulator). The time increases are largely due to the cost of advecting the additional tracers, together with expected increases in the microphysics, convection and large-scale cloud scheme. The peak memory usage at N96 resolution increases



205



at 0.8% per water tracer. However, at N216, there is no significant change to the peak memory when running with 23 water tracers compared to the cost of running the model at a higher resolution overall.

#### 2.3 Prescribed Region and Scaled-flux Water Tracers

In order to test the water tracer development, various experiments are run with prescribed region and scaled-flux water tracers. The surface evaporative flux for these water tracers ( $E_{wt}$ ) is set as

$$E_{wt}(i,j,t,i_{wt}) = \begin{cases} R_q^{sfc}(i,j,t,i_{wt}) E(i,j,t), & E(i,j,t) < 0\\ SF(i,j,t,i_{wt}) E(i,j,t), & E(i,j,t) \ge 0 \end{cases}$$
(4)

where *SF* is the scaling factor, *E* is the model's water evaporative flux, and the indices *i, j, t, i<sub>wt</sub>* indicate the fields are functions of longitude, latitude, time and water tracer number respectively.  $R_q^{sfc}$  is the ratio of water tracer to water specific humidity at the lowest atmosphere level and is used to calculate the amount of water tracer removed from the atmosphere during negative evaporation (i.e. condensation). The prescribed-region tracers are set up to separately track water evaporating from land, open ocean (including leads) and sea ice. For these tracers, *SF* is defined as the fractional area of the grid box covered by the surface from which water is being tagged. The prescribed water tracers are set up to ensure that all water in the model is tracked at all times (i.e. *SF* sums to 1 for each grid box and timestep). Note, here *SF* is a function of time due to the time evolving sea ice cover. The individual evaporative fluxes for each surface type (i.e. land, open ocean or sea ice) are used by the water tracers, rather than grid box mean values, to capture situations where the flux is in different directions for different surfaces at the same grid point. Currently, the water tracers use the mean land flux rather than considering the separate fluxes over different land surfaces as calculated in JULES.

The scaled-flux tracers, as proposed by Fiorella et al. (2021), are implemented following the approach of G24 which focusses on open-ocean sourced precipitation only and ensures that a closed water tracer budget is maintained. This involves using three water tracers to obtain the mass-weighted mean evaporative property of ocean sourced precipitation. The first two tracers sum to the total amount of ocean sourced precipitation, while the third tracer captures the land and sea ice sourced precipitation. The scaling factor for the three tracers is set to,

$$SF(i,j,t,1) = \begin{cases} \frac{X(i,j,t) - X_{lower}}{X_{upper} - X_{lower}}, & \text{over the open ocean} \\ 0, & \text{over land and sea ice} \end{cases}$$

$$SF(i,j,t,2) = \begin{cases} 1 - SF(i,j,t,1), & \text{over the open ocean} \\ 0, & \text{over land and sea ice} \end{cases}$$



215

220

225

230

235

240



$$SF(i,j,t,3) = \begin{cases} 0, & \text{over the open ocean} \\ 1, & \text{over the land and sea ice} \end{cases}$$
 (5)

where X is the evaporative property that is being tracked (e.g. source latitude, source SST), and constants  $X_{lower}$  and  $X_{upper}$  are lower and upper limits on X and are used to ensure SF stays within the range of 0 to 1. Therefore, the values of all the water tracers should always remain between 0 and the prognostic water amount and this is enforced in the model. As derived in G24, the mass-weighted mean evaporative property of ocean sourced precipitation ( $\overline{X}$ ) is then obtained using the precipitation fields of the first two tracers as follows,

$$\bar{X}(i,j,t) = \frac{P_{wt}(i,j,t,1)}{(P_{wt}(i,j,t,1) + P_{wt}(i,j,t,2))} \left( X_{upper} - X_{lower} \right) + X_{lower}$$
(6)

where  $P_{wt}(i, j, t, i_{wt})$  is the water tracer precipitation.

Both types of water tracers are set up in groups such that each group tracks all the water in the model. This allows adjustments to be made during the timestep to ensure that the sum of the water tracers in each group remains equal to the actual water in the model at each grid point. The adjustments are mainly required due to the non-linear transport scheme. The mixing ratios of the water tracers are adjusted in a manner that, importantly, does not impact on their ratios, following the same approach used in the ECHAM6 atmosphere model (G24). As these types of water tracers are adjusted locally to match the model's water fields, there is no need to use the OCF scheme to ensure global conservation following advection (as is done for normal water). This is because global conservation for these water tracers will be achieved indirectly through the local adjustment.

Short UM experiments were run with highly simplified prescribed-region tracers to initially test the code. These included a test with a group of two tracers with SF set to 1 for the 1st tracer and set to 0 for the 2nd tracer. It was confirmed that the 2nd tracer precipitation remained zero throughout the run and the 1st tracer matched the model's water field. Another test involved a group of two tracers with SF set to 0.5 for both tracers everywhere and it was checked that the precipitation field for the two tracers was equal to half the actual precipitation rate.

#### 2.4 Comparison between scaled flux and prescribed region water tracers

To further check the UM water tracer code, the comparison test between scaled flux and prescribed region water tracers of G24 was repeated for the UM. In this test, the prescribed region tracers are set to track open ocean evaporation from 10° latitude bands and the model is run for 15 months (including a three month spin up period). The mass weighted mean source



250

255

260



latitude for precipitation at each grid point is then calculated, assuming the source latitude of each 10° band is the mid-latitude of the band. This field is then compared to the same field calculated using the scaled flux water tracers (Fig. 2).

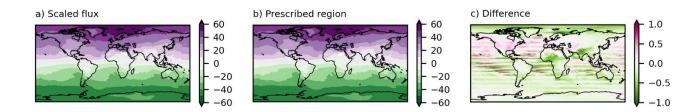


Figure 2. Mass-weighted mean of the open oceanic evaporative source latitude (in degrees) of annual mean precipitation evaluated from: a) the scaled flux water tracers; b) the prescribed region water tracers using 10° latitude bands. c) Difference (in degrees) between the scaled flux and prescribed region source latitude fields (a-b).

The difference is 1.8°. This provides confidence that both types of water tracers are working correctly in the UM. It also highlights the computational efficiency of the scaled flux method, which in this example, uses 3 tracers compared to 19 prescribed region tracers to get comparable results. The difference plot (Fig. 2c) shows clear latitudinal bands as was also found in the equivalent ECHAM6 experiment (G24), although the UM values are smaller. The stripey difference pattern is caused by the approximation of using the mid-latitude of each band in the prescribed region tracer calculation and reveals the improved precision of the scaled flux approach for this calculation. The precision of the prescribed region calculation can be improved by using more tracers with smaller latitude bands, but this makes the approach even more computationally expensive.

## 2.5 Model Experiment Setup

The water tracers are tested in an atmosphere-only historical run of the UM for the period 1979 to 2014. The 'N96' horizontal resolution of the UM is used which has 192 longitude points by 144 latitude points, with a mid-latitude resolution of 135km. There are 85 vertical levels with 50 levels below 18km and a fixed model lid at 85km above sea level. The simulation used the AMIP sea surface temperature and sea ice concentrations (Durack and Taylor, 2017) as surface boundary conditions. The scientific configuration was GAL9.0 and the UM version was 13.3.

The experiment included 23 water tracers: 1 normal water tracer; a group of 7 prescribed-region tracers (which together cover the entire Earth's surface); and 5 groups of scaled-flux tracers (which require 3 tracers in each group). Details are given in Table 1. Source longitude is found by tracking the sine and cosine of the source latitude to avoid problems with circular data as in G24. The source longitude can then be retrieved using the arctangent of the sine field divided by the cosine field. For



275

280



the purposes of this paper, the output from the two SH land water tracers (numbers 6 and 7) are combined to a single SH land 270 source tracer.

Water tracer	Type of water tracer	Details
number		
1	Normal water tracer	Comparable to model prognostic water field
2	Prescribed region	NH sea ice
3	Prescribed region	SH sea ice
4	Prescribed region	NH open ocean
5	Prescribed region	SH open ocean
6	Prescribed region	NH land
7	Prescribed region	SH land (north of 60 °S)
8	Prescribed region	Antarctica (land south of 60 °S)
9-11	Scaled flux	Source latitude, with $X_{lower} = -90^{\circ}$ , $X_{upper} = 90^{\circ}$
12-14	Scaled flux	sin (source longitude), with $X_{lower}$ = -1, $X_{upper}$ = 1
15-17	Scaled flux	cos (source longitude), with $X_{lower}$ = -1, $X_{upper}$ = 1
18-20	Scaled flux	Source SST, with $X_{lower}$ = -5 °C, $X_{upper}$ = 45 °C
21-23	Scaled flux	Wind speed in lowest grid box, with $X_{lower} = 0$ , $X_{upper} = 32 \text{ ms}^{-1}$

Table 1. Details of the water tracers used in the UM simulation. For the prescribed region tracers, the third column indicates the region of evaporation that is tracked by the tracer. For the scaled flux tracers, the third column states which evaporative property is being tracked.

The UM results were compared with a comparable simulation of the atmosphere model ECHAM6 (Stevens et al., 2013), forced with the same SST and sea ice fields. The ECHAM6 simulation uses a horizontal grid of 192 longitude points by 96 latitude points with 47 vertical levels reaching to 0.01 hPa (~100-110 km); therefore, it has a lower resolution latitudinally and vertically compared with the UM simulation. The water tracer set up for ECHAM6 follows that detailed in G24 which includes the same scaled flux tracers as in the UM simulation. As the ECHAM6 study focused on Antarctic precipitation sources, the prescribed-region fluxes are set up slightly differently to the UM study which is aiming to test the scheme globally.

The water tracers are initialised by setting the water tracer fields to the corresponding water field multiplied by *SF(i,j,t,i\_wt)*.

Due to the relatively short residence time of water in the atmosphere (Gimeno et al., 2021), the tracers spin up quickly. For the analysis presented here, the 30-year period of 1985-2014 is analysed.





## 3. Results

## 3.1 Prescribed region water tracers in the UM

The percentage of precipitation sourced from the different evaporative surface types, as obtained from the prescribed region 290 tracers, is shown in Fig. 3. As expected, the majority of precipitation is sourced directly from the ocean. The amount of precipitation sourced from sea ice sublimation is small and focused over spring/summer sea ice regions. The spatial pattern of the precipitation sourced directly from land (Fig. 3c and d) is comparable with similar maps from other studies: Findell et al. (2019, their figures 2b, d and f); van der Ent et al. (2014, their figure 2a) and Tuinenburg et al. (2020, their figure 4). The 295 precipitation over deserts is very low, but the source is still indicated here. In general, the amount of recycling over land increases downwind across continents. The largest recycling rates occur over the eastern part of Asia, with high rates also occurring in a band running northwest to southeast across central South America. Significant recycling is also diagnosed over parts of Africa and inland North America. There is a clear seasonal cycle in the land sourced precipitation (Fig. 4) with the largest values in the summer in each hemisphere, particularly in the NH, in agreement with other studies (Tuinenburg et al., 300 2020; Dirmeyer and Brubaker, 2007). In general, precipitation is sourced from the same hemisphere in which it falls. One exception is over the Indian monsoon region where precipitation includes a source from SH oceans, as also found in the water tracer study of Tharammal et al. (2023). Overall, the prescribed-region water tracer results look sensible.





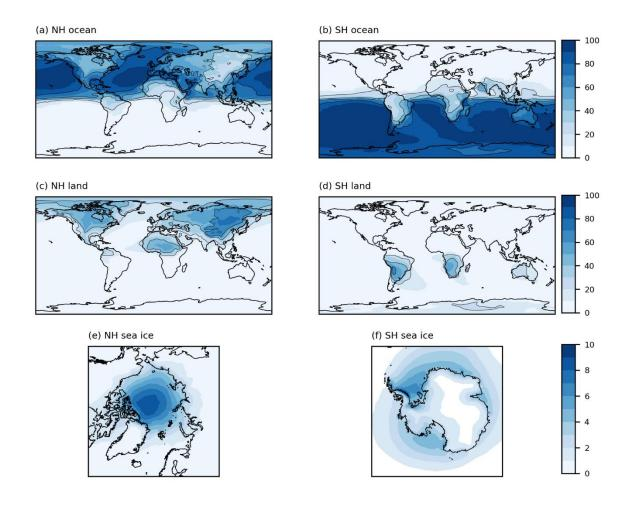


Figure 3: Percentage of annual mean precipitation from the 30-year UM simulation sourced from: a) NH open ocean evaporation (including leads); b) SH open ocean evaporation (including leads); c) NH land evapotranspiration; d) SH land evapotranspiration; e) NH sea ice sublimation; and f) SH sea ice sublimation.





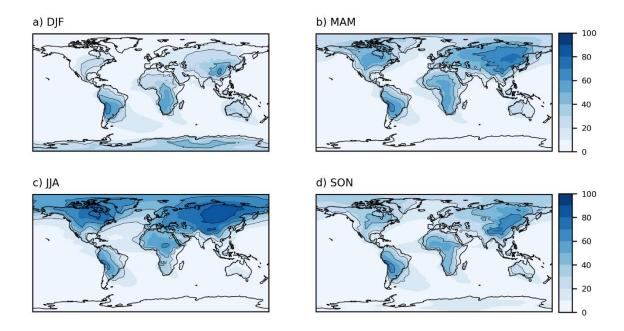


Figure 4. Percentage of precipitation from the 30-year UM simulation sourced from land for: a) December, January, February mean; b) March, April, May mean; c) June, July, August mean; and d) September, October, November mean.

## 3.2 Scaled-flux water tracers comparison between UM and ECHAM6

The UM water tracer code is further evaluated by comparing scaled-flux water tracers results with those from the ECHAM6 model. Figures 5-7 compares the mean evaporative source properties of latitude, longitude and SST for *ocean-sourced* precipitation for the two models. The large-scale patterns of the results from the two models are reassuringly very similar. The mean source latitude (Fig. 5) shows the expected pattern of precipitation being more locally sourced (in terms of latitude) in the tropics/sub-tropics and the source becoming more remote towards the poles. The dominant westerly storm tracks or easterly trade winds clearly impact on the mean source longitude at different latitudes in Fig. 6, with the mean precipitation source occurring upwind of where the precipitation falls. The mean source SST and latitude have similar spatial patterns as expected due to a strong correlation between the two fields (Fig. 7). Over the high altitudes of Antarctic and Greenland, both models show the precipitation is sourced remotely from relatively warm water compared with the source temperatures at surrounding lower heights. This is consistent with other findings that water vapour is sourced from relatively equatorwards/warm seas and then takes elevated pathways to reach the high elevations of the Antarctic Plateau (e.g. Noone and Simmonds, 2002; Sodemann and Stohl, 2009; Wang et al., 2020).

315





There are some interesting differences between the two models, which will be the subject of future work. These include the more southerly source of ocean water supplying precipitation over the Indian monsoon region and the more polewards source of precipitation over Antarctica and Greenland in the UM compared to ECHAM6 (Fig. 5). This demonstrates how water tracers can be a valuable diagnostic tool in highlighting contrasts in the hydrological cycle of different models.

330

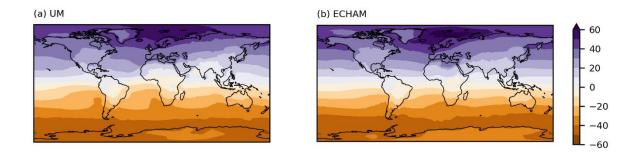


Figure 5: Mass-weighted mean of the open oceanic evaporative source latitude (in degrees) of annual mean precipitation for: a) UM; and b) ECHAM6.

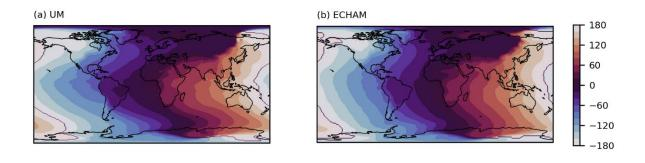


Figure 6: Mass-weighted mean of the open oceanic evaporative source longitude (in degrees) of annual mean precipitation for: a) UM; and b) ECHAM6.





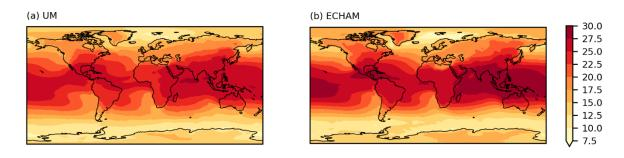


Figure 7: Mass-weighted mean of the open oceanic evaporative source SST (°C) of annual mean precipitation for: a) UM; and b) ECHAM6.

## 3.3 UM's global hydrological cycle derived from water tracers

To illustrate how water tracers can be used to gain a simplified view of the complex GCM, Fig. 8 shows the components of the model's global hydrological cycle that can be derived from the prescribed region tracers. The water tracers uniquely provide the amount of precipitation sourced separately from the land and the ocean (red arrows in Fig. 8). It is interesting to note that 40% of the land evaporative source precipitates out over ocean in the model. The hydrological cycle is completed in the model by the global runoff, which at steady state, should balance the net transport of atmospheric water from ocean to land (52 x 10<sup>3</sup> km<sup>3</sup> yr<sup>-1</sup>). The continental precipitation recycling ratio, as defined by van der Ent et al. (2010) as the percentage of continental precipitation that is land sourced, is 35% (as derived from the water tracer values in Fig. 8). This is slightly lower than the range of estimates from other present day studies, including 38 - 43% (Findell et al., 2019), 36% (van der Ent et al., 2014) and 51% (Tuinenburg et al., 2020).



360

365

370

375



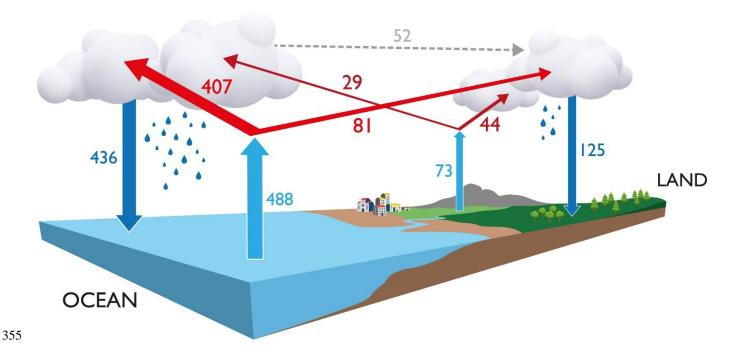


Figure 8: Global hydrological cycle fluxes (in 10<sup>3</sup> km<sup>3</sup> yr<sup>-1</sup>) derived from the prescribed region water tracer precipitation fields. The separate land and ocean sources of both the annual mean land and ocean precipitation are shown from the 30-year model simulation. The red arrows indicate the additional information provided by the water tracers compared to standard diagnostics. The grey dashed arrow shows the net ocean to land flux of atmospheric water. Sea ice is included in the ocean component for this diagram.

The precipitation source values in Fig.8 can be compared to the model's standard net evaporative diagnostics to estimate the accuracy level of the water tracers. The net evaporation over land is  $72.29 \times 10^3 \text{ km}^3 \text{ yr}^{-1}$  compared to the water tracer land source amount of  $73.09 \times 10^3 \text{ km}^3 \text{ yr}^{-1}$ . There is a subtle difference in the definition of these two fields; the net evaporation includes the impact of negative evaporation which is not included in Fig. 8. However, preliminary investigations suggest that this is not sufficient to explain the  $0.8 \times 10^3 \text{ km}^3 \text{ yr}^{-1}$  difference. Therefore, the 1% difference can be viewed as an estimate of the accuracy of the water tracers for tracking total land evaporation. The difference between the global total water tracer precipitation and the actual precipitation diagnostic is very small ( $7 \times 10^{-8} \%$ ), indicating that the water tracers are tracking all the water in the model to a high degree of accuracy but that the split between separate tracers introduces some numerical error as to be expected.

This technical paper is not intended as a scientific assessment of the UM's hydrological cycle. However, comparing Fig. 8 to observational and reanalysis based global estimates (e.g. Trenberth et al., 2007; Rodell et al., 2015; Koutsoyiannis, 2020) suggests the model's hydrological cycle is too strong with ocean precipitation and evaporation being too large. This has been stated as a common model problem and a well-known issue for the UM (Williams et al., 2017; Walters et al., 2019). However,





Abbott et al. (2019) found a large range of global ocean precipitation ( $320 - 460 \times 10^3 \text{ km}^3 \text{ yr}^{-1}$ ) and evaporation ( $350 - 510 \times 10^3 \text{ km}^3 \text{ yr}^{-1}$ ) estimates and there are many challenges in observing these fields (Dorigo et al., 2021). Indeed, the UM values do compare well with those given in Allan et al. (2020).

#### 4. Conclusions

Numerical water tracers have been successfully implemented in the UM, which track water through the following processes: surface evaporation, large-scale advection, surface exchange, boundary layer mixing, large-scale precipitation, cloud microphysics and convection. The implementation has been shown to track water to a high degree of precision, with the difference between the prognostic water and water tracer specific humidity remaining less than 10<sup>-10</sup> kg kg<sup>-1</sup> at the end of each timestep in a 35-year simulation. This has not been a trivial task. For example, it has required the water tracers being 'plumbed' through the entire microphysics and convection schemes to correctly track the transport and phase changes of water in these schemes. The code implementation for the normal water tracer has passed the Met Office's review and approval process and is now included in the code trunk. This helps ensure that the water tracer code will have longevity and will remain up to date with the underlying model. The new water tracer capability is relatively efficient compared to the standard run time of the UM, with one water tracer increasing the run time by 3-4%.

390

395

Tests have been carried out using prescribed region and scaled-flux water tracers in a historical simulation and the results have been compared with the ECHAM6 model. Both types of water tracers produce sensible distributions and the scaled-flux water tracer results are comparable to ECHAM6, which provides confidence in the new UM development. There are some interesting differences in the source properties between the models in certain regions (e.g. over South Asia, Greenland and Antarctic) and the water tracers will be used in future projects to investigate the causes of these differences. The comparison highlights that water tracers provide a valuable diagnostic tool in inter-model comparisons. It has also been demonstrated that the water tracers can be used to assess the model in an integrated and simplified manner in global hydrological cycle diagrams, including providing unique information.

from

400

The scaled-flux water tracers offer an efficient method to estimate the mean source location of the world's precipitation directly from the model. For tracing all evaporation (rather than open-ocean evaporation as done in this paper), seven tracers would be required (2 for latitude, 4 for longitude plus 1 normal water tracer), increasing the UM run time by only ~22% at the N96 resolution. Therefore, including these tracers in standard climate model runs is feasible and would allow predicted changes to source locations to be easily assessed.

405

Work has recently been completed to add water tracers to the land surface model, JULES, which is used with the UM. The next step for this continuing development is to add isotopic fractionation processes to the UM and JULES so that water isotopes

https://doi.org/10.5194/egusphere-2024-3824 Preprint. Discussion started: 12 February 2025

© Author(s) 2025. CC BY 4.0 License.



410

EGUsphere Preprint repository

can be modelled, which is the ultimate aim for this work. Modelled water isotopes can be compared with measured values in vapour and precipitation, including those preserved in ice cores, which will provide new opportunities for model evaluation work both for present day and paleoclimates. To conclude, the new water tracer UM development is a valuable tool in

understanding the hydrological cycle in past, present and future simulations.

Code and data availability

Due to intellectual property rights restrictions, we cannot provide the source code for the UM. The Met Office Unified Model is available for use under licence. A number of research organisations and national meteorological services use the UM in collaboration with the Met Office to undertake basic atmospheric process research, produce forecasts, develop the UM code, and build and evaluate Earth system models. For further information on how to apply for a licence, see http://www.metoffice.gov.uk/research/approach/modelling-systems/unified-model. The UM and/or JULES code branch(es) used in the publication have not all been submitted for review and inclusion in the UM/JULES trunk or released for general use. However, the UM/JULES code used has been made available to reviewers; reviewers can contact the topical editor for details of accessing the code.

The UM water tracer precipitation data is available in the Centre for Environmental Data Analysis (CEDA) archive: https://catalogue.ceda.ac.uk/uuid/10ae416c4ccb4a90bdb5da0bbf68d4f9/

425 Author contributions

AM managed the water tracer code development in the UM and wrote the scientific related code. SW wrote the technical infrastructure code in the UM. AM carried out the UM run and analysis, whilst the ECHAM6 run and analysis were done by QG. GL carried out the timing tests. LS instigated and continues to manage the project to add water tracers and isotopes to the UKESM. All authors were involved in planning and discussing the code development. AM wrote the paper with

contributions from all co-authors.

**Competing interests** 

430

The authors declare that they have no conflict of interest.





# Acknowledgements

We thank the Met Office's Simulation Systems and Deployment Team for their support during this development and the various scientists and software scientists that reviewed the code during the Met Office's review and approval process. We acknowledge use of the Monsoon2 system, a collaborative facility supplied under the Joint Weather and Climate Research Programme, a strategic partnership between the Met Office and the Natural Environment Research Council.

## **Financial support**

The UM code development was supported by the European Union's Horizon 2020 research and innovation programme under grant agreement no. 820970 (TiPES project). Alison McLaren and Louise Sime were also supported by: NERC UK Polar Research Expertise for Science and Society: PRESCIENT (grant number NE/Y006178/1); NERC The Sensitivity of the West Antarctic Ice Sheet to +2C: SWAIS2C (grant number NE/X009386/1) and NERC SURface FluxEs In AnTarctica: SURFEIT (grant number NE/X009319/1). Qinggang Gao was supported by the European Union's Horizon 2020 research and innovation programme under Marie Sklodowska-Curie grant agreement no. 955750 (DEEPICE project).

#### References

450

455

Abbott, B.W., Bishop, K., Zarnetske, J.P., Minaudo, C., Chapin III, F.S., Krause, S., Hannah, D.M., Conner, L., Ellison, D., Godsey, S.E., Plont, S, Marçais, J., Kolbe, T., Huebner, A., Frei, R.J., Hampton, T., Gu, S., Buhman, M., Sayedi, S.S, Ursache, O., Chapin, M., Henderson, K.D., and Pinay, G.: Human domination of the global water cycle absent from depictions and perceptions, Nature Geoscience, 12, 533-540, https://doi.org/10.1038/s41561-019-0374-y, 2019.

Allan, R.P., Barlow, M., Byrne, M.P., Cherchi, A., Douville, H., Fowler, H.J., Gan, T.Y., Pendergrass, A.G., Rosenfeld, D., Swann, A.L., Wilcox, L.J. and Zolina, O.: Advances in understanding large-scale responses of the water cycle to climate change, Ann. NY Acad. Sci., 1472, 49–75, https://doi.org/10.1111/nyas.14337, 2020.

460 Best, M. J., Pryor, M., Clark, D. B., Rooney, G. G., Essery, R. L. H., Ménard, C. B., Edwards, J. M., Hendry, M. A., Porson, A., Gedney, N., Mercado, L. M., Sitch, S., Blyth, E., Boucher, O., Cox, P. M., Grimmond, C. S. B., and Harding, R. J.: The



470

485



Joint UK Land Environment Simulator (JULES), model description—Part 1: energy and water fluxes. Geosci. Model Dev., 4, 677–699, https://doi.org/10.5194/gmd-4-677-2011, 2011.

- Bosilovich, M.G., and Schubert, S.D.: Water Vapor Tracers as Diagnostics of the Regional Hydrologic Cycle, J. Hydrometeor., 3, 149–165, https://doi.org/10.1175/1525-7541(2002)003<0149:WVTADO>2.0.CO;2, 2002.
  - Brown, A., Milton, S., Cullen, M., Golding, B., Mitchell, J. and Shelly, A.: Unified modeling and prediction of weather and climate: A 25-year journey, B. Am. Meteorol. Soc., 93, 1865–1877, https://doi.org/10.1175/BAMS-D-12-00018.1, 2012.
- Cauquoin, A., Werner, M. and Lohmann, G.: Water isotopes–climate relationships for the mid-Holocene and preindustrial period simulated with an isotope-enabled version of MPI-ESM, Clim. Past, 15, 1913–1937, https://doi.org/10.5194/cp-15-1913-2019, 2019.
- Clark, D. B., Mercado, L. M., Sitch, S., Jones, C. D., Gedney, N., Best, M. J., Pryor, M., Rooney, G. G., Essery, R. L. H., Blyth, E., Boucher, O., Harding, R. J., Huntingford, C., and Cox, P. M.: The Joint UK Land Environment Simulator (JULES), model description—Part 2: carbon fluxes and vegetation dynamics, Geosci. Model Dev., 4, 701–722, https://doi.org/10.5194/gmd-4-701-2011, 2011
- Delaygue, G., Masson, V., Jouzel, J., Koster, R.D. and Healy, R.J.: The origin of Antarctic precipitation: a modelling approach, Tellus, 52B, 19-36, http://doi.org/10.3402/tellusb.v52i1.16079, 2000.
  - Dirmeyer, P.A. and Brubaker, K.L.: Characterization of the global hydrologic cycle from a back-trajectory analysis of atmospheric water vapor, J. Hydrometeor., 8, 20–37, https://doi.org/10.1175/JHM557.1, 2007.
  - Dominguez, F., Hu, H. and Martinez, J.A.: Two-layer dynamic recycling model (2L-DRM): Learning from moisture tracking models of different complexity, J. Hydrometeor., 21, 3–16, https://doi.org/10.1175/JHM-D-19-0101.1, 2020.
- Dorigo, W., Dietrich, S., Aires, F., Brocca, L., Carter, S., Cretaux, J., Dunkerley, D., Enomoto, H., Forsberg, R., Güntner, A., Hegglin, M. I., Hollmann, R., Hurst, D. F., Johannessen, J. A., Kummerow, C., Lee, T., Luojus, K., Looser, U., Miralles, D. G., Pellet, V., Recknagel, T., Vargas, C. R., Schneider, U., Schoeneich, P., Schröder, M., Tapper, N., Vuglinsky, V., Wagner, W., Yu, L., Zappa, L., Zemp, M., & Aich, V.: Closing the water cycle from observations across scales: Where do we stand?, Bull. Amer. Meteor. Soc., 102, E1897–E1935, https://doi.org/10.1175/BAMS-D-19-0316.1, 2021.





- 495 Durack, P.J. and Taylor, K.E.: PCMDI AMIP SST and sea-ice boundary conditions version 1.1.2. Earth System Grid Federation [dataset], https://doi.org/10.22033/ESGF/input4MIPs.1161, 2017
- Findell, K.L., Keys, P.W., Van Der Ent, R.J., Lintner, B.R., Berg, A. and Krasting, J.P.: Rising temperatures increase importance of oceanic evaporation as a source for continental precipitation, J. Climate, 32, 7713–7726, https://doi.org/10.1175/JCLI-D-19-0145.1, 2019.
  - Fiorella, R.P., Siler, N., Nusbaumer, J. and Noone, D.C.: Enhancing understanding of the hydrological cycle via pairing of process-oriented and isotope ratio tracers, Journal of Advances in Modeling Earth Systems, 13, e2021MS002 648, https://doi.org/10.1029/2021MS002648, 2021.
  - Gao, Q., Sime, L.C., McLaren, A.J., Bracegirdle, T.J., Capron, E., Rhodes, R.H., Steen-Larsen, H.C., Shi, X. and Werner, M.: Evaporative controls on Antarctic precipitation: an ECHAM6 model study using innovative water tracer diagnostics, The Cryosphere, 18, 683–703, https://doi.org/10.5194/tc-18-683-2024, 2024.
- 510 Gimeno, L., Stohl, A., Trigo, R.M., Dominguez, F., Yoshimura, K., Yu, L., Drumond, A., Durán-Quesada, A.M. and Nieto, R.: Oceanic and terrestrial sources of continental precipitation, Rev. Geophys., 50, RG4003, https://doi.org/10.1029/2012RG000389, 2012.
- Gimeno, L., Eiras-Barca, J., Durán-Quesada, A.M., Dominguez, F., van der Ent, R., Sodemann, H., Sánchez-Murillo, R., Nieto, R. and Kirchner, J.W.: The residence time of water vapour in the atmosphere, Nat. Rev. Earth Environ., 558–569, https://doi.org/10.1038/s43017-021-00181-9, 2021.
- Gordon, C., Cooper, C., Senior, C.A., Banks, H., Gregory, J.M., Johns, T.C., Mitchell, J.F. and Wood, R.A.: The simulation of SST, sea ice extents and ocean heat transports in a version of the Hadley Centre coupled model without flux adjustments, Clim. Dynam., 16, 147-168, https://doi.org/10.1007/s003820050010, 2000.
  - Joussaume, S., Sadourny, R. and Jouzel, J.: A general circulation model of water isotope cycles in the atmosphere, Nature, 311, 24–29, https://doi.org/10.1038/311024a0, 1984.
- Koster, R., Jouzel, J., Suozzo, R., Russell, G., Broecker, W., Rind, D. and Eagleson, P.: Global sources of local precipitation as determined by the NASA/GISS GCM, Geophys. Res. Lett., 13, 121–124, http://doi.org/10.1029/GL013i002p00121, 1986.



530

540



Koutsoyiannis, D.: Revisiting the global hydrological cycle: is it intensifying?, Hydrol. Earth Syst. Sci., 24, 3899–3932, https://doi.org/10.5194/hess-24-3899-2020, 2020.

Met Office Simulation Systems Working Practices: https://metoffice.github.io/simulation-systems/, last access: 14 August 2024.

Noone, D. and Simmonds, I.: Annular variations in moisture transport mechanisms and the abundance of δ18O in Antarctic snow, J. Geophys. Res., 107(D24), 4742, https://doi.org/10.1029/2002JD002262, 2002.

Noone, D. and Sturm, C.: Comprehensive dynamical models of global and regional water isotope distributions, in: Isoscapes: Understanding movement, pattern, and process on Earth through isotope mapping, edited by: West, J., Bowen, G., Dawson, T., Tu, K., Springer, Dordrecht, 195-219, https://doi.org/10.1007/978-90-481-3354-3\_10, 2010.

Numaguti, A.: Origin and recycling processes of precipitating water over the Eurasian continent: Experiments using an atmospheric general circulation model, J. Geophys. Res., 104(D2), 1957-1972, https://doi.org/10.1029/1998JD200026, 1999.

Nusbaumer, J. and Noone, D.: Numerical evaluation of the modern and future origins of atmospheric river moisture over the West Coast of the United States, J. Geophys. Res.: Atmospheres, 123, 6423–6442, https://doi.org/10.1029/2017JD028081, 2018.

Nusbaumer, J., Wong, T.E., Bardeen, C. and Noone, D.: Evaluating hydrological processes in the Community Atmosphere Model Version 5 (CAM5) using stable isotope ratios of water, J. Adv. Model. Earth Syst., 9, 949–977, https://doi.org/10.1002/2016MS000839, 2017.

Oger, S., Sime, L., and Holloway, M.: Decoupling of  $\delta$ 18O from surface temperature in Antarctica in an ensemble of Historical simulations, EGUsphere [preprint], https://doi.org/10.5194/egusphere-2023-2735, 2023.

Pope, V.D., Gallani, M.L., Rowntree, P.R. and Stratton, R.A.: The impact of new physical parametrizations in the Hadley Centre climate model: HadAM3, Clim. Dynam., 16, 123-146, https://doi.org/10.1007/s003820050009, 2000.

Rockström, J., Mazzucato, M., Andersen, L.S., Fahrländer, L.S., and Gerten, D.: Why we need a new economics of water as a common good, Nature, 615, 794-797, https://doi.org/10.1038/d41586-023-00800-z, 2023.





Rodell, M., Beaudoing, H. K., L'Ecuyer, T. S., Olson, W. S., Famiglietti, J. S., Houser, P. R., Adler, R., Bosilovich, M. G., Clayson, C. A., Chambers, D., Clark, E., Fetzer, E. J., Gao, X., Gu, G., Hilburn, K., Huffman, G. J., Lettenmaier, D. P., Liu, W. T., Robertson, F. R., Schlosser, C. A., Sheffield, J., & Wood, E. F.: The observed state of the water cycle in the early twenty-first century, J. Climate, 28, 8289–8318, https://doi.org/10.1175/JCLI-D-14-00555.1, 2015.

565

570

Sellar, A. A., Jones, C. G., Mulcahy, J. P., Tang, Y., Yool, A., Wiltshire, A., O'Connor, F. M., Stringer, M., Hill, R., Palmieri, J., Woodward, S., de Mora, L., Kuhlbrodt, T., Rumbold, S. T., Kelley, D. I., Ellis, R., Johnson, C. E., Walton, J., Abraham, N. L., Andrews, M. B., Andrews, T., Archibald, A. T., Berthou, S., Burke, E., Blockley, E., Carslaw, K., Dalvi, M., Edwards, J., Folberth, G. A., Gedney, N., Griffiths, P. T., Harper, A. B., Hendry, M. A., Hewitt, A. J., Johnson, B., Jones, A., Jones, C. D., Keeble, J., Liddicoat, S., Morgenstern, O., Parker, R. J., Predoi, V., Robertson, E., Siahaan, A., Smith, R. S., Swaminathan, R., Woodhouse, M. T., Zeng, G., and Zerroukat, M.: UKESM1: Description and evaluation of the U.K. Earth System Model, J. Adv. Model. Earth Sy., 11, 4513–4558, https://doi.org/10.1029/2019MS001739, 2019.

Sodemann, H., and Stohl, A.: Asymmetries in the moisture origin of Antarctic precipitation, Geophys. Res. Lett., 36, L22803, https://doi.org/10.1029/2009GL040242, 2009.

Stevens, B., Giorgetta, M., Esch, M., Mauritsen, T., Crueger, T., Rast, S., Salzmann, M., Schmidt, H., Bader, J., Block, K., Brokopf, R., Fast, I., Kinne, S., Kornblueh, L., Lohmann, U., Pincus, R., Reichler, T., and Roeckner, E.: Atmospheric component of the MPI-M Earth System Model: ECHAM6, J. Adv. Model. Earth Sy., 5, 146–172, https://doi.org/10.1002/jame.20015, 2013.

Tharammal, T., Bala, G. and Nusbaumer, J.M.: Sources of water vapor and their effects on water isotopes in precipitation in the Indian monsoon region: a model-based assessment, Sci Rep 13, 708, https://doi.org/10.1038/s41598-023-27905-9, 2023.

Tindall, J. C., Valdes, P. J., and Sime, L. C.: Stable water isotopes in HadCM3: Isotopic signature of El Niño—Southern Oscillation and the tropical amount effect, J. Geophys. Res., 114, D04111, https://doi.org/10.1029/2008JD010825, 2009.

Trenberth, K. E., Smith, L., Qian, T., Dai, A., & Fasullo, J.: Estimates of the Global Water Budget and Its Annual Cycle Using Observational and Model Data, J. Hydrometeor., 8, 758–769, https://doi.org/10.1175/JHM600.1, 2007.

590

Tuinenburg, O.A., Theeuwen, J.J.E. and Staal, A.: High-resolution global atmospheric moisture connections from evaporation to precipitation, Earth Syst. Sci. Data, 12, 3177–3188, https://doi.org/10.5194/essd-12-3177-2020, 2020.





- Valdes, P. J., Armstrong, E., Badger, M. P. S., Bradshaw, C. D., Bragg, F., Crucifix, M., Davies-Barnard, T., Day, J. J.,
  Farnsworth, A., Gordon, C., Hopcroft, P. O., Kennedy, A. T., Lord, N. S., Lunt, D. J., Marzocchi, A., Parry, L. M., Pope, V.,
  Roberts, W. H. G., Stone, E. J., Tourte, G. J. L., and Williams, J. H. T.: The BRIDGE HadCM3 family of climate models:
  HadCM3@Bristol v1.0, Geosci. Model Dev., 10, 3715–3743, https://doi.org/10.5194/gmd-10-3715-2017, 2017.
- van der Ent, R.J., Savenije, H.H.G., Schaefli, B. and Steele-Dunne, S.C.: Origin and fate of atmospheric moisture over continents, Water Resour. Res., 46, W09525, https://doi.org/10.1029/2010WR009127, 2010.
  - van der Ent, R.J., Wang-Erlandsson, L., Keys, P.W. and Savenije, H.H.G.: Contrasting roles of interception and transpiration in the hydrological cycle–Part 2: Moisture recycling, Earth Syst. Dynam., 5, 471–489, https://doi.org/10.5194/esd-5-471-2014.
- Kavier, P., Willett, M., Graham, T., Earnshaw, P., Copsey, D., Marzin, C., Sellar, A., Ackerley, D., Alves, O., Blockley, E., Bodas-Salcedo, A., Bushell, A., Butchart, N., Calvert, D., Cho, J-A., Copsey, D., de Burgh-Day, C., Edwards, J., Earnshaw, P., Furtado, K., Field, P., Guiavarch, C., Hardy, S., Harris, C., Heywood, K., Heming, J., Hendon, H., Hewitt, H., Hyder, P., Hyun, Y-K., Hyun, S-H., Ineson, S., Jones, R., Kim, J., Kim, K-Y., Klingaman, N., Levine, R., Lee, S-M., Lekakou, K., Lock, A., Martin, G., Mathiot, P., Megann, A., Meijers, A., Moon, J-Y., Morgenstern, O., North, R., Nurser, G., Park, Y-H., Regayre,
- 610 L., Roberts, M., Rodriguez, J., Ridley, J., Rawlins, R., Sinha, B., Shin, B., Semple, A., Storkey, D., Stephens, D., Shim, T., Tomassini, L., Tsushima, Y., Titley, H., Tennant, W., Varma, V., Vellinga, M., Weedon, G., Williams, K., Yang, Y-M., Zhao, M., Zhou, X., and Zhu, H.: Assessment of the Met Office Global Coupled model version 4 (GC4) configurations, The Forecasting Research Technical Report No: 661, Met Office, https://doi.org/10.62998/uzui3766, 2024.
- Walters, D., Baran, A. J., Boutle, I., Brooks, M., Earnshaw, P., Edwards, J., Furtado, K., Hill, P., Lock, A., Manners, J., Morcrette, C., Mulcahy, J., Sanchez, C., Smith, C., Stratton, R., Tennant, W., Tomassini, L., Van Weverberg, K., Vosper, S., Willett, M., Browse, J., Bushell, A., Carslaw, K., Dalvi, M., Essery, R., Gedney, N., Hardiman, S., Johnson, B., Johnson, C., Jones, A., Jones, C., Mann, G., Milton, S., Rumbold, H., Sellar, A., Ujiie, M., Whitall, M., Williams, K., and Zerroukat, M.: The Met Office Unified Model Global Atmosphere 7.0/7.1 and JULES Global Land 7.0 configurations, Geosci. Model Dev.,
  12, 1909–1963, https://doi.org/10.5194/gmd-12-1909-2019, 2019.
  - Wang, H., Fyke, J. G., Lenaerts, J. T. M., Nusbaumer, J. M., Singh, H., Noone, D., Rasch, P. J., and Zhang, R.: Influence of sea-ice anomalies on Antarctic precipitation using source attribution in the Community Earth System Model, The Cryosphere, 14, 429–444, https://doi.org/10.5194/tc-14-429-2020, 2020.





Werner, M., Heimann, M., and Hoffmann, G.: Isotopic composition and origin of polar precipitation in present and glacial climate simulations. Tellus B: Chemical and Physical Meteorology, 53, 53–71. https://doi.org/10.3402/tellusb.v53i1.16539, 2001.

Willett, M., Roach, L. A., Dörr, J., Holmes, C. R., Massonnet, F., Blockley, E. W., Notz, D., and Rackow, T.: GAL9 documentation paper, in preparation, 2024.

Williams, K. D., Copsey, D., Blockley, E. W., Bodas-Salcedo, A., Calvert, D., Comer, R., Davis, P., Graham, T., Hewitt, H. T., Hill, R., Hyder, P., Ineson, S., Johns, T. C., Keen, A. B., Lee, R. W., Megann, A., Milton, S. F., Rae, J. G. L., Roberts, M.
J., Scaife, A. A., Schiemann, R., Storkey, D., Thorpe, L., Watterson, I. G., Walters, D. N., West, A., Wood, R. A., Woollings, T., and Xavier, P. K.: The Met Office Global Coupled Model 3.0 and 3.1 (GC3.0 and GC3.1) Configurations, J. Adv. Model. Earth Sy., 10, 357–380, https://doi.org/10.1002/2017MS001115, 2017.

Wood, N., Staniforth, A., White, A., Allen, T., Diamantakis, M., Gross, M., Melvin, T., Smith, C., Vosper, S., Zerroukat, M., and Thuburn, J.: An inherently mass-conserving semi-implicit semi-Lagrangian discretization of the deep-atmosphere global non-hydrostatic equations, Q. J. Roy. Meteorol. Soc., 140, 1505–1520, https://doi.org/10.1002/qj.2235, 2014.

Zerroukat, M. and Allen, T.: On the monotonic and conservative transport on overset/Yin-Yang grids, J. Comput. Phys., 302, 285–299, https://doi.org/10.1016/j.jcp.2015.09.006, 2015.